Publishing House
AKAPIT

COMPUTER METHODS IN MATERIALS SCIENCE
Informatyka w Technologii Materiałów

Vol. 18, 2018, No. 2

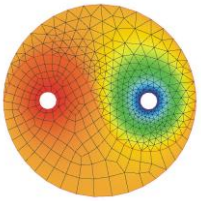

THE MIXED FEM FOR ANALYSIS OF QUANTUM-DOT SYSTEMS BASED ON GRADIENT THEORY

JAN SLADEK[1*], VLADIMIR SLADEK[1], MIROSLAV REPKA[1], SLAVOMIR HRCEK[2]

[1]Institute of Construction and Architecture, Slovak Academy of Sciences, 84503 Bratislava, Slovakia
[2]Faculty of Mechanical Engineering, University of Zilina, 01026 Zilina, Slovakia
[*]Corresponding author: jan.sladek@savba.sk

Abstract

The QD nanostructures are analyzed under a thermal load. The dimensions of the QDs are of the same order as the material length scale. Therefore, the gradient elasticity theory should be applied to account for the size-dependent behavior of such nano-sized QDs. Since governing equations contain higher order derivatives than in conventional approaches the C^1-elements are required for approximation of primary fields in the FEM. The mixed FEM are developed here, where C^0 continuous interpolation is applied independently for displacement and displacement gradients. The kinematic constraints between strains and displacements are satisfied by collocation at some cleverly chosen internal points in elements. A unit cell of Indium Arsenide QD in a finite sized Gallium Arsenide (GaAs) substrate is analysed.

Key words: Mixed FEM, Gradient theory, Thermo-piezoelectricity, Quantum dots, Thermal shock

1. INTRODUCTION

Quantum Dots (QDs) offer revolutionary advantages in their wide range of applications such as solid state lighting, power efficient LEDs for superior performance in displays and photovoltaics, solar cells, quantum computing and medical imaging. Quantum dots are tiny nanocrystals of a semiconducting material with characteristic length of several nanometers and they are buried into piezoelectric matrix. The QDs can be tuned during manufacturing to emit any colour of light from the same material simply by changing the dot size. Due to lattice mismatch or thermal expansion difference between the QD and matrix both elastic and electric fields are induced in this system (Bimberg et al., 1998). A reliable analysis of these fields are crucial to the design and fabrication of such structures. In the first stage, semi-coupled computational approaches were applied to analyze QD systems. In the first step strains are computed from pure elasticity equations. Then, these results are used to compute electric field (Davies et al., 1994; Davies, 1998; Pryor et al., 1997; Liao et al., 1999; Benabbas et al., 1996; Grundmann et al., 1995; Jogai, 2001). Later, Pan (2002a, 2002b) demonstrated that the semi-coupled model could produce large errors for both the elastic and electric fields. Therefore, the fully coupled approach should always be used to model QD systems.

Liu et al. (2008) showed that shape and the area density of the QDs can be controlled by varying the growth parameters such as the growth temperature, growth rate, annealing progress and the growth interruption. Thermal expansion coefficient and pyroelectric parameter can also play a very important role in tuning of QDs. Hence temperature can also be considered as another tuning parameter. The QDs can work at extreme thermal conditions, therefore, it is important to understand the steady state and transient effects of temperature on the QD system. Giazotto et al. (2006) analyzed QDs in low temperature regime, and Chen et al. (2008) considered higher temperature. Patil and Melnik (2009) applied the thermo-piezoelectricity theory for QDs under stationary boundary conditions.

 ISSN 1641-8581

The material length scale is comparable with the dimensions of the QDs. Then, the classical thermo-piezoelectricity theory cannot be applied since it neglects the interaction of material microstructure, and the results are size-independent. The atomistic models have the extremely high requirements on computer memory and there are difficulties with application to real problems. Advanced continuum theories with size effect ability seem to be convenient for our QD system. The former Mindlin's theory (Mindlin, 1964) with two length scales has been simplified by Aifantis (1984), Altan and Aifantis (1992), Askes and Aifantis (2011) in elasticity. This simplified Aifantis theory is extended here to thermo-piezoelectricity.

This paper presents, for the first time, application of the gradient theory of thermo-piezoelectricity for 3D analyses of QDs under transient thermal conditions. The FEM in gradient theory requires using C1-continuous elements to guarantee the continuity of the problem variables and their derivates at the element boundaries. It is not an easy task to develop C1 continuous elements. It seems to be more convenient to construct a mixed formulation for our gradient theory. Therefore, the mixed FEM is developed to solve boundary value problems. It uses the C0 continuous interpolation independently for displacement and displacement gradients. The kinematic constraints between strains and displacements are satisfied by collocation at some cleverly chosen internal points in elements (Bishay & Atluri, 2012). The present collocation method reduces the number of DOFs with respect to the Lagrangian approach.

Numerical results obtained by the present gradient formulation are compared with those obtained by the classical coupled thermo-piezoelectric theory, and the influence of the size effect parameter is discussed.

2. THE GRADIENT THEORY FOR THERMO-ELECTRO-MECHANICAL FIELDS

The inherent initial strain induces electric and elastic fields in the QD system. This initial strain is produced by the lattice mismatch. A periodic distribution of QDs in the matrix is considered and a representative volume element (RVE) illustrated in figure 1 (top) is numerically analyzed.

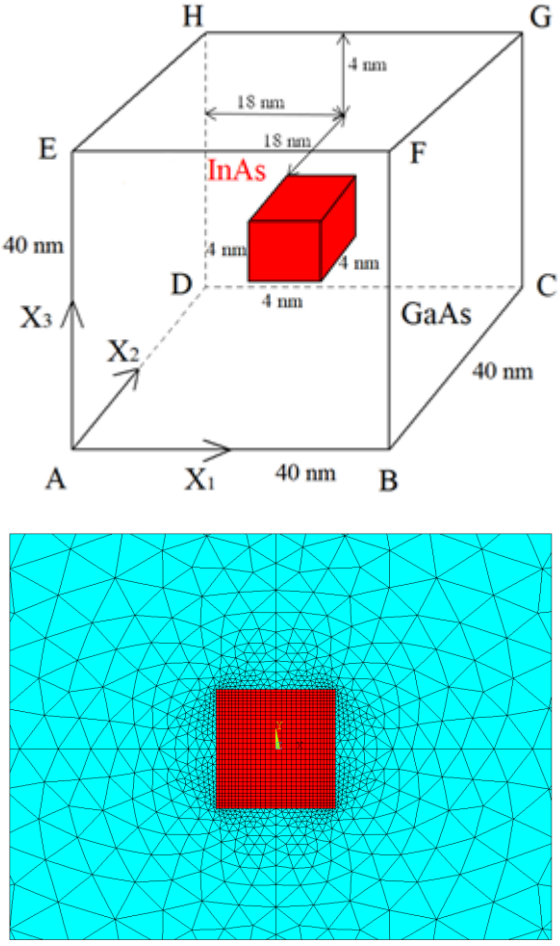

Fig. 1. *A unit cell of QD piezoelectric structure (top) with FE mesh around the QD (bottom).*

It is considered thermo-piezoelectricity, where the heat generation caused by mechanical/electric fields is very weak (Patil & Melnik, 2009). However, the stresses and electrical displacements can be influenced by temperature variation. For typical material coefficients the changes of the electromagnetic fields can be assumed to be immediate, or in other words the electromagnetic fields can be considered quasi-static (Parton & Kudryavtsev, 1988).

We define kinematic equations for strain tensor ε_{ij}, the electric field vector E_j and the temperature gradient vector β_j by:

$$\begin{aligned} \varepsilon_{ij} &= \frac{1}{2}\left(u_{i,j} + u_{j,i}\right) \\ E_j &= -\phi_{,j} \\ \beta_j &= \theta_{,j} \end{aligned} \tag{1}$$

where: u_i, ϕ, θ - displacements, the electric potential and the temperature, respectively.

The total strain is given as a sum of elastic and thermal strains and eigestrains:

$$\varepsilon_{ij}^{e} = \varepsilon_{ij} - \varepsilon_{ij}^{*} - \alpha_{ij}\theta$$
$$\varepsilon_{ij}^{*} = \chi \frac{a_m - a_{QD}}{a_{QD}} \qquad (2)$$
$$\chi = \begin{cases} 1, & \text{in QD} \\ 0, & \text{in matrix} \end{cases}$$

where: α_{ij} - the coefficients of linear thermal expansion, ε_{ij}^{*} - the eigenstrain tensor, a_m, a_{OD} - lattice constants of the matrix and QD, respectively.

The lattice mismatch inside the matrix is neglected and homogeneous eigenstrains inside the QD are assumed (Patil & Melnik, 2009). The strain-gradient tensor is defined as:

$$\eta_{ijk} = \varepsilon_{ij,k} = \frac{1}{2}\left(u_{i,jk} + u_{j,ik}\right) \qquad (3)$$

Then, the elastic strain gradients are defined as:

$$\eta_{ijk}^{e} = \varepsilon_{ij,k}^{e} = \left(\varepsilon_{ij} - \alpha_{ij}\theta\right)_{,k} \qquad (4)$$

where: $\varepsilon_{ij,k}^{*} = 0$.

The gradient theory is applied to the piezoelectric solids under thermal loads in this work. The deformation energy density in gradient theory for thermo-piezoelectricity is written as (Toupin & Gazis, 1963; DiVincenzo, 1986)

$$\mathcal{U}\left(\boldsymbol{\varepsilon}, \nabla\boldsymbol{\varepsilon}, \mathbf{E}, \theta, \boldsymbol{\beta}\right) = \frac{1}{2}c_{ijkl}\varepsilon_{ij}\varepsilon_{kl}$$
$$+\frac{1}{2}g_{ijklmn}\eta_{ijk}\eta_{lmn} + \frac{1}{2}h_{ij}E_iE_j + \frac{1}{2}\kappa_{ij}\beta_i\beta_j \qquad (5)$$
$$-e_{ijk}\varepsilon_{ij}E_k - \gamma_{ij}\varepsilon_{ij}\theta - c_{ijkl}\varepsilon_{ij}\varepsilon_{kl}^{*} + p_iE_i\theta$$

where: c_{ijkl}, e_{ijkl}, h_{ij}, p_i, κ_{ij} - the material elastic, piezoelectric, dielectric, pyroelectric and thermal conductivity tensors in the thermo-piezoelectric medium, respectively. The high-order elastic tensor is denoted by g_{ijklmn}. The stress-temperature modulus γ_{ij} can be expressed as $\gamma_{ij} = c_{ijkl}\alpha_{kl}$, where α_{kl} is the linear thermal expansion coefficient

The constitutive equations for the Cauchy stress σ_{ij}, the higher-order stress τ_{ijk}, the electric displacement D_i and heat flux vector λ_i can be obtained from the deformation energy density as:

$$\sigma_{ij}(\mathbf{x},t) = \frac{\partial\mathcal{U}}{\partial\varepsilon_{ij}} \qquad (6)$$
$$= c_{ijkl}\left[\varepsilon_{kl}(\mathbf{x},t) - \varepsilon_{kl}^{*}(\mathbf{x},t)\right] - e_{kij}E_k(\mathbf{x},t) - \gamma_{ij}\theta(\mathbf{x},t)$$

$$\tau_{ijk}(\mathbf{x},t) = \frac{\partial\mathcal{U}}{\partial\eta_{ijk}} = g_{ijklmn}\eta_{lmn}(\mathbf{x},t) \qquad (7)$$

$$D_i(\mathbf{x},t) = \frac{\partial\mathcal{U}}{\partial E_i} = \qquad (8)$$
$$e_{ijk}\varepsilon_{jk}(\mathbf{x},t) + h_{ij}E_j(\mathbf{x},t) + p_i\theta(\mathbf{x},t)$$

$$\tau_{ijk}\lambda_i(\mathbf{x},t) = -\frac{\partial\mathcal{U}}{\partial\beta_i} = -\kappa_{ij}\beta_j(\mathbf{x},t) \qquad (9)$$

where: t - the time.

One can see that in this uncoupled thermo-piezoelectricity the heat flux is independent of the elastic and electrical fields. Constitutive equations (6) – (9) for material with cubic symmetry can be written in matrix form, using the reduced Voigt notation, as:

$$\begin{Bmatrix} \sigma_{11} \\ \sigma_{22} \\ \sigma_{33} \\ \sigma_{23} \\ \sigma_{13} \\ \sigma_{12} \end{Bmatrix} = \begin{bmatrix} c_{11} & c_{12} & c_{12} & 0 & 0 & 0 \\ c_{12} & c_{11} & c_{12} & 0 & 0 & 0 \\ c_{12} & c_{12} & c_{11} & 0 & 0 & 0 \\ 0 & 0 & 0 & c_{44} & 0 & 0 \\ 0 & 0 & 0 & 0 & c_{44} & 0 \\ 0 & 0 & 0 & 0 & 0 & c_{44} \end{bmatrix} \begin{Bmatrix} \varepsilon_{11}^{r} \\ \varepsilon_{22}^{r} \\ \varepsilon_{33}^{r} \\ 2\varepsilon_{23}^{r} \\ 2\varepsilon_{13}^{r} \\ 2\varepsilon_{12}^{r} \end{Bmatrix} - \begin{bmatrix} 0 & 0 & 0 \\ 0 & 0 & 0 \\ 0 & 0 & 0 \\ e_{14} & 0 & 0 \\ 0 & e_{14} & 0 \\ 0 & 0 & e_{14} \end{bmatrix} \begin{Bmatrix} E_1 \\ E_2 \\ E_3 \end{Bmatrix} - \begin{Bmatrix} \gamma_{11} \\ \gamma_{22} \\ \gamma_{33} \\ 0 \\ 0 \\ 0 \end{Bmatrix} \theta \qquad (10)$$

$$\begin{Bmatrix} D_1 \\ D_2 \\ D_3 \end{Bmatrix} = \begin{bmatrix} 0 & 0 & 0 & e_{14} & 0 & 0 \\ 0 & 0 & 0 & 0 & e_{14} & 0 \\ 0 & 0 & 0 & 0 & 0 & e_{14} \end{bmatrix} \begin{Bmatrix} \varepsilon_{11} \\ \varepsilon_{22} \\ \varepsilon_{33} \\ 2\varepsilon_{23} \\ 2\varepsilon_{13} \\ 2\varepsilon_{12} \end{Bmatrix} + \begin{bmatrix} h_{11} & 0 & 0 \\ 0 & h_{11} & 0 \\ 0 & 0 & h_{11} \end{bmatrix} \begin{Bmatrix} E_1 \\ E_2 \\ E_3 \end{Bmatrix} + \begin{Bmatrix} p_1 \\ p_1 \\ p_1 \end{Bmatrix} \theta \tag{11}$$

$$\begin{Bmatrix} \lambda_1 \\ \lambda_2 \\ \lambda_3 \end{Bmatrix} = - \begin{bmatrix} \kappa_{11} & 0 & 0 \\ 0 & \kappa_{11} & 0 \\ 0 & 0 & \kappa_{11} \end{bmatrix} \begin{Bmatrix} \beta_1 \\ \beta_2 \\ \beta_3 \end{Bmatrix} \tag{12}$$

$$\boldsymbol{\tau} = l^2 \mathbf{C}\boldsymbol{\eta}^r - l^2 \mathbf{C}\boldsymbol{\alpha}\boldsymbol{\beta} \tag{13}$$

where:

$$\begin{Bmatrix} \gamma_{11} \\ \gamma_{22} \\ \gamma_{33} \end{Bmatrix} = \begin{bmatrix} c_{11} & c_{12} & c_{12} \\ c_{12} & c_{11} & c_{12} \\ c_{12} & c_{12} & c_{11} \end{bmatrix} \begin{Bmatrix} \alpha_{11} \\ \alpha_{11} \\ \alpha_{11} \end{Bmatrix} \tag{14}$$

and $\varepsilon_{ij}^r = \varepsilon_{ij} - \varepsilon_{ij}^*$

It is considered above that higher-order elastic parameters g_{ijklmn} are proportional to the conventional elastic stiffness coefficients c_{klmn} by the internal length material parameter l (Gitman et al., 2010; Liang & Shen, 2013; Yaghoubi et al., 2017).

Equations (10)-(12) can be written in a compact form as:

$$\begin{aligned} \boldsymbol{\sigma} &= \mathbf{C}\boldsymbol{\varepsilon}^r - \mathbf{Z}\mathbf{E} - \boldsymbol{\gamma}\theta \\ \mathbf{D} &= \mathbf{Z}^T\boldsymbol{\varepsilon} + \mathbf{G}\mathbf{E} + \mathbf{p}\theta \\ \boldsymbol{\lambda} &= -\boldsymbol{\kappa}\boldsymbol{\beta} \end{aligned} \tag{15}$$

Recently, the authors have derived the governing equations for gradient thermo-piezoelectricity without higher-order effects in the heat conduction equation (Sladek et al., 2017). In uncoupled thermoelasticity, the temperature distribution is independent of the elastic and electrical fields. Then, the governing equations derived earlier for the elastic and electrical fields are formally unchanged:

$$\begin{aligned} \sigma_{ij,j}(\mathbf{x},t) - \tau_{ijk,jk}(\mathbf{x},t) &= 0 \\ D_{k,k}(\mathbf{x},t) &= 0 \end{aligned} \tag{16}$$

Above governing equations have to be supplemented by the heat conduction equation:

$$\lambda_{i,i}(\mathbf{x},t) - \rho c\dot{\theta}(\mathbf{x},t) = 0 \tag{17}$$

where: ρ, c - the mass density and specific heat, respectively. Dots over a quantity indicate time derivatives.

Essential and natural boundary conditions (b.c.) can be prescribed in the present theory:

1. Essential b.c.:

$$\begin{aligned} &u_i(\mathbf{x}) = \bar{u}_i \ \text{ on } \ \Gamma_u, \ \Gamma_u \subset \Gamma \\ &s_i(\mathbf{x}) = \bar{s}_i \ \text{ on } \ \Gamma_s, \ \Gamma_s \subset \Gamma \\ &\phi_i(\mathbf{x}) = \bar{\phi}_i \ \text{ on } \ \Gamma_\phi, \ \Gamma_\phi \subset \Gamma \\ &\theta(\mathbf{x},t) = \bar{\theta}(\mathbf{x},t) \quad \text{ on } \ \Gamma_\theta, \ \Gamma_\theta \subset \Gamma \end{aligned} \tag{18}$$

2. Natural b.c.

$$\begin{aligned} &t_i(\mathbf{x}) = \bar{t}_i \ \text{ on } \ \Gamma_t, \ \Gamma_t \cup \Gamma_u = \Gamma, \Gamma_t \cap \Gamma_u = \varnothing \\ &R_i(\mathbf{x}) = \bar{R}_i \text{ on } \ \Gamma_R, \ \Gamma_R \cup \Gamma_S = \Gamma, \Gamma_t \cap \Gamma_u = \varnothing \\ &S(\mathbf{x}) = \bar{S}(\mathbf{x}) \ \text{ on } \ \Gamma_S, \Gamma_S \cup \Gamma_\phi = \Gamma, \Gamma_S \cap \Gamma_\phi = \varnothing \\ &\Lambda(\mathbf{x},t) = \lambda_i(\mathbf{x},t) n_i(\mathbf{x}) = \bar{\Lambda}(\mathbf{x},t) \text{ on } \Gamma_\lambda, \Gamma_\lambda \cup \Gamma_\theta = \Gamma \end{aligned} \tag{19}$$

where:

$$s_i := \frac{\partial u_i}{\partial \mathbf{n}}, \qquad R_i := n_k n_j \tau_{ijk} \tag{20}$$

and the traction vector, and the electric charge are defined as:

$$t_i := n_j \left(\sigma_{ij} - \tau_{ijk,k} \right) - \frac{\partial \rho_i}{\partial \boldsymbol{\pi}} + \sum_c \left\| \rho_i(\mathbf{x}^c) \right\| \delta(\mathbf{x} - \mathbf{x}^c) \tag{21}$$

$$S := n_k D_k \tag{22}$$

with ρ_i: = $n_k \pi_j \tau ijk$, $\delta(\mathbf{x})$ being the Dirac delta function and π_j is the Cartesian component of the unit tangent vector on Γ.

The jump at a corner (x^c) on the oriented boundary contour Γ is defined as:

$$\left\| \rho_i(\mathbf{x}^c) \right\| := \rho_i(\mathbf{x}^c + 0) - \rho_i(\mathbf{x}^c - 0) \tag{23}$$

Initial conditions for temperature is assumed as:

$$\theta(\mathbf{x},t)\big|_{t=0} = \theta(\mathbf{x},0) \quad \text{ in } \Omega \tag{24}$$

3. THE MIXED FINITE ELEMENT METHOD

The weak-form of a boundary value problem in gradient thermo-piezoelectricity can be derived from the principle of virtual work, where the variation of

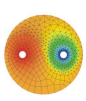

the electro-elastic Gibbs free energy has to be equal to the work of the external generalized forces on generalized displacements

$$\int_{\Omega}\left(\lambda_i\delta\theta_{,i}-\rho c\dot{\theta}\delta\theta\right)d\Omega=\int_{\Gamma_\lambda}\bar{\Lambda}\delta\theta d\Gamma \tag{25}$$

$$\begin{aligned}&\int_{\Omega}\left(\sigma_{ij}\delta u_{i,j}+\tau_{ijk}\delta u_{i,jk}+D_k\delta\phi_{,k}\right)d\Omega\\&=\int_{\Gamma_t}\bar{t}_i\delta u_i d\Gamma+\int_{\Gamma_R}\bar{R}_i\delta s_i d\Gamma+\int_{\Gamma_S}\bar{S}\delta\phi d\Gamma\end{aligned} \tag{26}$$

where overbar is used for prescribed boundary values.

Furthermore, it is assumed that:

$$\delta\theta|_{\Gamma-\Gamma_\lambda}=0 \qquad \delta u_i|_{\Gamma-\Gamma_t}=0$$
$$\delta s_i|_{\partial V-\Gamma_R}=0 \qquad \delta\phi|_{\Gamma-\Gamma_S}=0$$

The presence of strain gradients in the deformation energy density requires C^1 continuous interpolations of displacements. The mixed FEM is developed here, where C^0 continuous interpolation is applied independently for displacement and displacement gradients. The kinematic constraints (1) between strains and displacements are satisfied by collocation at some cleverly chosen internal points in elements (Bishay & Atluri, 2012; Dong & Atluri, 2011).

The mechanical displacements and electric potential in each element are expressed in terms of nodal values and shape functions:

$$\mathbf{u}=N_u\left(\xi_1,\xi_2,\xi_3\right)\mathbf{q}_u \tag{27}$$

$$\phi=N_\phi\left(\xi_1,\xi_2,\xi_3\right)\mathbf{q}_\phi \tag{28}$$

where: $\mathbf{q}_u$, $\mathbf{q}_\phi$, Ni(ξ_1, ξ_2, ξ_3,) - nodal displacements, electric potential and shape functions, respectively.

The strain and electric intensity vector can be expressed from the kinematic equation (1) and approximation (27) as:

$$\boldsymbol{\varepsilon}=\begin{bmatrix}\varepsilon_{11}\\ \varepsilon_{22}\\ \varepsilon_{33}\\ 2\varepsilon_{23}\\ 2\varepsilon_{13}\\ 2\varepsilon_{12}\end{bmatrix}=\begin{bmatrix}\partial_1 & 0 & 0\\ 0 & \partial_2 & 0\\ 0 & 0 & \partial_3\\ 0 & \partial_3 & \partial_2\\ \partial_3 & 0 & \partial_1\\ \partial_2 & \partial_1 & 0\end{bmatrix}\begin{bmatrix}u_1\\ u_2\\ u_3\end{bmatrix}=\mathbf{B}_u(\xi_1,\xi_2,\xi_3)\mathbf{q}_u$$

$$\mathbf{s}=\partial_1\begin{bmatrix}u_1\\ u_2\\ u_3\end{bmatrix}n_1+\partial_2\begin{bmatrix}u_1\\ u_2\\ u_3\end{bmatrix}n_2+\partial_3\begin{bmatrix}u_1\\ u_2\\ u_3\end{bmatrix}n_3=\mathbf{B}_s(\xi_1,\xi_2,\xi_3)\mathbf{q}_u$$

$$-\mathbf{E}=-\begin{bmatrix}E_1\\ E_2\\ E_3\end{bmatrix}=\begin{bmatrix}\partial_1\\ \partial_2\\ \partial_3\end{bmatrix}\phi=\mathbf{B}_\phi(\xi_1,\xi_2,\xi_3)\mathbf{q}_\phi$$

$$\boldsymbol{\beta}=\begin{Bmatrix}\partial_1\\ \partial_2\\ \partial_3\end{Bmatrix}\mathbf{N}(\xi_1,\xi_2,\xi_3)\mathbf{q}_\theta=\mathbf{B}_\theta(\xi_1,\xi_2,\xi_3)\mathbf{q}_\theta \tag{29}$$

Beside using the mechanical displacement approximation (27) we use also independent approximation of strains. These approximations in local coordinates can be written as (Bishay & Atluri, 2012):

$$\hat{\boldsymbol{\varepsilon}}^{In}=\mathbf{A}\left(\xi_1,\xi_2,\xi_3\right)\boldsymbol{\alpha} \tag{30}$$

Where: $\boldsymbol{\alpha}$ - undetermined coefficients.

For 3D 8-node brick element the polynomial function matrix can be given by:

$$\begin{aligned}&\mathbf{A}\left(\xi_1,\xi_2,\xi_3\right)\\&=\left[1\quad \xi_1\quad \xi_2\quad \xi_3\quad \xi_1\xi_2\quad \xi_1\xi_3\quad \xi_2\xi_3\quad \xi_1\xi_2\xi_3\right]\end{aligned}$$

Bishay and Atluri (2012) recommended to select the collocations at Gauss quadrature points. Then, one can write:

$$\hat{\boldsymbol{\varepsilon}}^{In}\left(\boldsymbol{\xi}^c,\boldsymbol{\alpha}\right)=\hat{\boldsymbol{\varepsilon}}\left(\boldsymbol{\xi}^c,\mathbf{q}_u\right) \tag{31}$$

Where: $\boldsymbol{\xi}^c=\left(\xi_1^c,\xi_2^c,\xi_3^c\right)$ - collocation points.

Collocation is performed for all components at the same points. Strains are collocated at the 8 points and comparing equations (30) and (29) one can write

$$\mathbf{A}\boldsymbol{\alpha}=\mathbf{B}_u\mathbf{q}_u \tag{32}$$

Substituting $\boldsymbol{\alpha}$ from (32) into equation (30), the independent strains can be expressed by nodal displacements

$$\hat{\boldsymbol{\varepsilon}}^{In}=\mathbf{A}(\xi_1,\xi_2,\xi_3)\mathbf{L}\mathbf{q}_u \tag{33}$$

where: $\mathbf{L}=\mathbf{A}^{-1}\mathbf{B}_u$

The independent strain gradients in local coordinate system are given as:

$$\begin{aligned}\hat{\boldsymbol{\eta}}^{In}&=\begin{bmatrix}\partial_1\\ \partial_2\\ \partial_3\end{bmatrix}\hat{\boldsymbol{\varepsilon}}^{\ddot{I}n}=\begin{bmatrix}\partial_1\\ \partial_2\\ \partial_3\end{bmatrix}\mathbf{A}\left(\xi_1,\xi_2,\xi_3\right)\boldsymbol{\alpha}\\&=\mathbf{A}^*\left(\xi_1,\xi_2,\xi_3\right)\boldsymbol{\alpha}=\mathbf{A}^*\left(\xi_1,\xi_2,\xi_3\right)\mathbf{L}\mathbf{q}_u\end{aligned} \tag{34}$$

To simplify the FEM equations further, we consider vanishing pyroelectric coefficient. The varia-

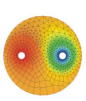

tions of the primary field variables can be also expressed in terms of the variations of the nodal values. Thus, the variational statements, equations (25) and (26), can be rewritten as:

$$\begin{aligned}&-\int_{\Omega}\{\delta\mathbf{q}_\theta\}^T\mathbf{B}_\theta^T(\xi^c)\boldsymbol{\kappa}\mathbf{B}_\theta(\xi^c)\{\mathbf{q}_\theta\}d\Omega\\&-\int_{\Omega}\{\delta\mathbf{q}_\theta\}^T\mathbf{B}_\theta^T(\xi^c)\rho c\mathbf{N}(\xi^c)\{\dot{\mathbf{q}}_\theta\}d\Omega\\&=\{\delta\mathbf{q}_\theta\}^T\int_{\Gamma_\lambda}\bar{\Lambda}\mathbf{N}d\Gamma\end{aligned}\tag{35}$$

Substituting this into the functional (26) we get:

$$\begin{aligned}&\int_{\Omega}\mathbf{L}^T\{\delta\mathbf{q}_u\}^T\mathbf{A}^T(\xi^c)\mathbf{C}\mathbf{A}(\xi^c)\mathbf{L}\{\mathbf{q}_u\}d\Omega\\&+\int_{\Omega}\mathbf{L}^T\{\delta\mathbf{q}_u\}^T\mathbf{A}^T(\xi^c)\mathbf{Z}\mathbf{B}_\phi(\xi^c)\{\mathbf{q}_\phi\}d\Omega\\&-\int_{\Omega}\mathbf{L}^T\{\delta\mathbf{q}_u\}^T\mathbf{A}^T(\xi^c)\boldsymbol{\gamma}\mathbf{N}(\xi^c)\{\theta\}d\Omega\\&+\int_{\Omega}\mathbf{A}^{*T}\mathbf{L}^T(\xi^c)\{\delta\mathbf{q}_u\}^T l^2\mathbf{C}\mathbf{A}^*(\xi^c)\mathbf{L}\{\mathbf{q}_u\}d\Omega\\&-\int_{\Omega}\mathbf{A}^{*T}\mathbf{L}^T(\xi^c)\{\delta\mathbf{q}_u\}^T l^2\mathbf{C}\boldsymbol{\alpha}\mathbf{B}_\theta(\xi^c)\{\mathbf{q}_\theta\}d\Omega\\&+\int_{\Omega}\mathbf{B}_\phi^T\{\delta\mathbf{q}_\phi\}^T\mathbf{Z}^T\mathbf{B}_u(\xi^c)\{\mathbf{q}_u\}d\Omega\\&-\int_{\Omega}\mathbf{B}_\phi^T\{\delta\mathbf{q}_\phi\}^T\mathbf{G}\mathbf{B}_\phi(\xi^c)\{\mathbf{q}_\phi\}d\Omega\\&+\int_{\Omega}\mathbf{B}_\phi^T\{\delta\mathbf{q}_\phi\}^T p\mathbf{N}(\xi^c)\{\mathbf{q}_\theta\}d\Omega\\&=\{\delta\mathbf{q}_u\}^T\int_{\Gamma_t}\bar{\mathbf{T}}\mathbf{N}d\Gamma+\{\delta\mathbf{q}_u\}^T\int_{\Gamma_R}\bar{\mathbf{R}}\mathbf{B}_s d\Gamma\\&+\{\delta\mathbf{q}_\phi\}^T\int_{\Gamma_S}\bar{\mathbf{S}}\mathbf{N}d\Gamma\end{aligned}\tag{36}$$

Where: **C**, **Z**, **G** - matrices of elastic, piezoelectric and dielectric constants, respectively.

Since the variational forms (35) and (36) are, respectively, valid for any arbitrary $\delta\mathbf{q}_\theta$, $\delta\mathbf{q}_u$, and $\delta\mathbf{q}_\phi$ satisfying the Dirichlet boundary conditions, the following system of ordinary differential equations and algebraic equations is obtained:

$$\begin{aligned}&-\int_{\Omega}\mathbf{B}_\theta^T(\xi^c)\boldsymbol{\kappa}\mathbf{B}_\theta(\xi^c)\{\mathbf{q}_\theta\}d\Omega\\&-\int_{\Omega}\mathbf{B}_\theta^T(\xi^c)\rho c\mathbf{N}(\xi^c)\{\dot{\mathbf{q}}_\theta\}d\Omega=\int_{\Gamma_\lambda}\bar{\Lambda}\mathbf{N}d\Gamma\end{aligned}\tag{37}$$

$$\begin{aligned}&\int_{\Omega}\mathbf{L}^T\mathbf{A}^T(\xi^c)\mathbf{C}\mathbf{A}(\xi^c)\mathbf{L}\{\mathbf{q}_u\}d\Omega\\&+\int_{\Omega}\mathbf{L}^T\mathbf{A}^T(\xi^c)\mathbf{Z}\mathbf{B}_\phi(\xi^c)\{\mathbf{q}_\phi\}d\Omega\\&-\int_{\Omega}\mathbf{L}^T\mathbf{A}^T(\xi^c)\boldsymbol{\gamma}\mathbf{N}(\xi^c)\{\theta\}d\Omega\\&+\int_{\Omega}\mathbf{A}^{*T}\mathbf{L}^T(\xi^c)l^2\mathbf{C}\mathbf{A}^*(\xi^c)\mathbf{L}\{\mathbf{q}_u\}d\Omega\\&-\int_{\Omega}\mathbf{A}^{*T}\mathbf{L}^T(\xi^c)l^2\mathbf{C}\boldsymbol{\alpha}\mathbf{B}_\theta(\xi^c)\{\mathbf{q}_\theta\}d\Omega=\int_{\Gamma_t}\bar{\mathbf{T}}\mathbf{N}d\Gamma+\int_{\Gamma_R}\bar{\mathbf{R}}\mathbf{B}_s d\Gamma\end{aligned}\tag{38}$$

$$\begin{aligned}&\int_{\Omega}\mathbf{B}_\phi^T\mathbf{Z}^T\mathbf{B}_u(\xi^c)\{\mathbf{q}_u\}d\Omega-\int_{\Omega}\mathbf{B}_\phi^T\mathbf{G}\mathbf{B}_\phi(\xi^c)\{\mathbf{q}_\phi\}d\Omega\\&+\int_{\Omega}\mathbf{B}_\phi^T p\mathbf{N}(\xi^c)\{\mathbf{q}_\theta\}d\Omega=\int_{\Gamma_S}\bar{\mathbf{S}}\mathbf{N}d\Gamma\end{aligned}\tag{39}$$

4. NUMERICAL RESULTS

The representative volume element (RVE) in figure 1 is assumed to have a cubic geometry with side length of 40 nm, and a cubic QD with side length of a = 4 nm is embedded in it. The top surface of the InAs QD is 4 nm from the top surface of the matrix. Material properties of correspond to the InAs (Glazov & Pashinkin, 2000). The substrate is made of GaAs, whose properties are:

c_{11} = 118.8 GPa, c_{12} = 54 GPa, c_{44} = 59.4 GPa

e_{14} = -0.16 C/m^2, h_{11} = 0.1346×10^{-9} C^2/Nm^2,

α = 5.1 ×10^{-6} deg^{-1}, c = 350 J/kgdeg,

κ_{12} = 0.044 W/m, ρ = 5.32×10^3 kg/m^3.

The lattice constant differences define the eigenstrains are $\varepsilon_{11}^* = \varepsilon_{22}^* = \varepsilon_{33}^*$ = 0.07. The pyroelectric coefficient p_1 is not considered in the numerical analyses since this quantity can be neglected.

The four side faces of the matrix are fixed along their normal direction, the bottom face is fixed along its normal direction, and the upper surface is free of tractions. Lateral sides and bottom side of the matrix cube are thermally isolated. Temperature is prescribed on the top. All surfaces have vanishing normal component of electric displacement, except for the bottom side, where a vanishing electric potential is prescribed. One can write the following boundary conditions for the InAs/GaAs quantum dot structure (figure 1):

On surfaces BCGF and ADHE: $u_1 = 0$, $t_2 = t_3 = 0$, $D_2 = 0$, $q = 0$.

ABFE and DCGH: $u_3 = 0$, $t_1 = t_2 = 0$, $\phi = 0$, $q = 0$.

EFGH: $t_3 = 0$, $t_1 = t_2 = 0$, $D_3 = 0$, $\theta = \theta_0$.

On the interface between InAs and GaAs, the continuity of primary fields has to be satisfied, namely:

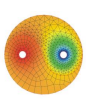

$u_i^{CM} = u_i^{cQD}$, $\phi^m = \phi^{OD}$, $\theta^m = \theta^{OD}$

as well as the reciprocity of traction vector, electric displacement and heat flux:

$$T_i^m + T_i^{QD} = 0, \qquad D_i^m + D_i^{QD} = 0, \qquad q^m + q^{QD} = 0$$

A 3D FEM model was created by constructing the geometry and meshing it using 195,696 elements corresponding to 339,117 nodes as shown in figure 1. Mixed FEM results can be verified by ANSYS if the structural material parameter is vanishing (classical theory).

The material length scale parameter is considered as $l = 0.5\times10^{-9}$ m (Majdoub et al., 2008). To illustrate its influence on strains, there are considered more values of the intrinsic material characteristics. This material parameter represents microstructural size, and therefore it has to be smaller than the size of the QD, a. As such, the admissible dimensionless ratio l/a should be restricted to the range from 0 to 1.

To test the computer code we have analyzed the QD structure under a thermal load to be 500°C if l = 0. The variation of the strain component ε_{11} along X_1 direction (passing the QD center) and electric potential ϕ along X_3 (aligned with the edge of the QD at X_1 = 18 nm and X_2 = 22 nm) is presented in figure 2. One can observe excellent agreement between the mixed FEM and ANSYS results with error less than 1% for both the strain and electric potential.

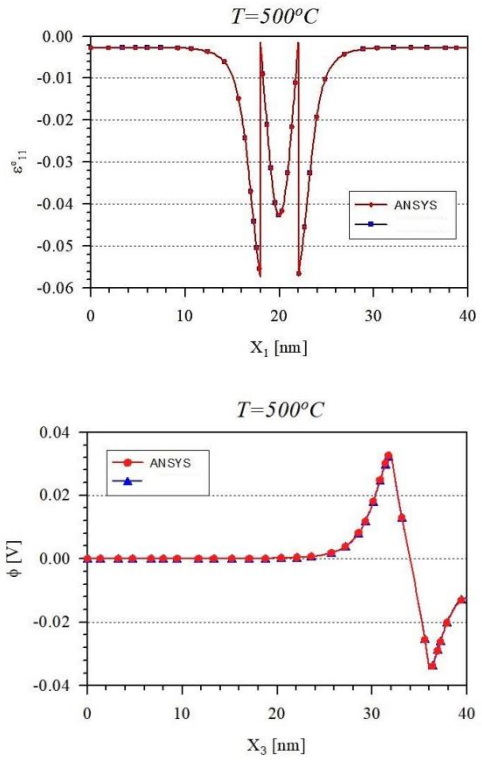

Fig. 2. *Elastic strain component ε_{11} along X_1-direction (passing the QC center) (top) and the potentials ϕ along X_3 at X_1 = 18 nm and X_2 = 22 nm (bottom).*

Figure 3 shows the influence of the material characteristic length, l, on the normal strains and at a constant temperature (250°C). As the size-effect parameter, l, increases, the magnitude of the strains decreases significantly and therefore the corresponding system becomes stiffer. As the QD size gets smaller with respect to the parameter l, the strains decrease. This provides a new opportunity for designing stiffer QD nanostructure by decreasing the size of the QDs to the level that experiences this size effect. Furthermore, size-effect eliminates the sharp transitions of the strains at the interfaces of the boundaries, reducing the field concentration, and thus making the structure safer.

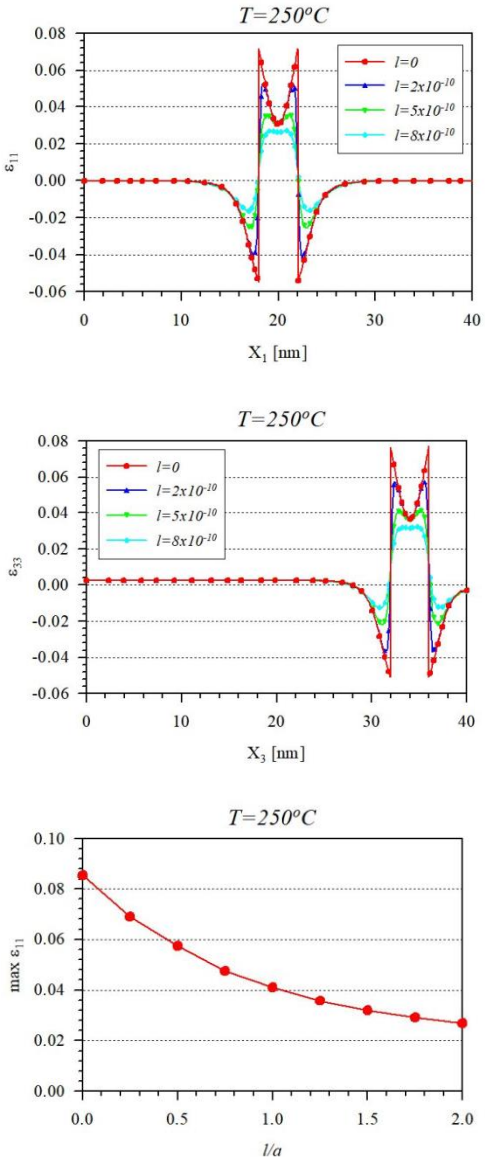

Fig. 3. *Variation of normal strains (top) along X_3-direction (passing the QD center), for various size effect parameters l.*

Next, a transient thermal load is considered. A 500°C temperature shock load on the upper surface of the matrix is prescribed. The variations of strain

components ε_{11} and ε_{33} along the X_1 - and X_3 - directions, respectively, are presented in figure 4 and figure 5.

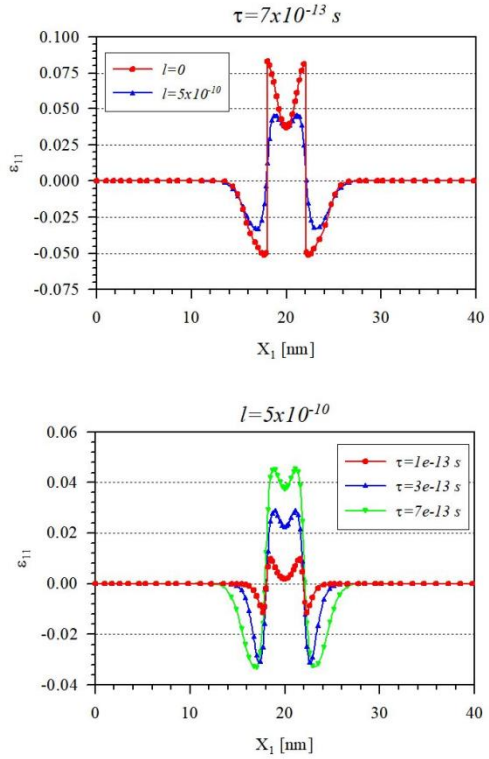

Fig. 4. *The variation of strain component ε_{11} along the X_1 - direction (passing the QD center) under thermal shock load.*

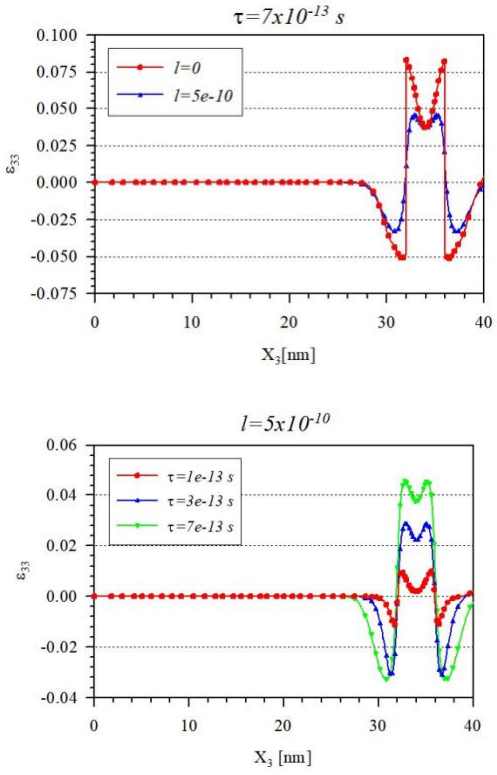

Fig. 5. *The variation of strain component ε_{33} along X_3-direction (passing the QD center) under thermal shock load.*

The line $l = 0$ corresponds to classical elasticity at time $t = 7\times10^{-13}$ s. One can observe that induced strains are varying with time significantly. If material structure scale parameter is increasing, the stiffness of system groves and the induced strains are reduced. These trends need to be carefully considered when the nanostructure is under thermal dynamic loads

5. CONCLUSIONS

The 3D mixed finite element model has been developed for thermo-piezoelectric analysis of the effect of a thermal shock load on a QD embedded in a piezoelectric substrate. The periodic QD array is replaced by a representative volume element (RVE), which is analyzed by the gradient theory of thermo-piezoelectricity. It was observed that the largest magnitudes of the induced strain fields are within or near the QD regions. Then, the effect of the lattice mismatch dominates there. It was also found that size-effect parameter increases the stiffness and reduces the induced strains if the size of QDs is smaller. The dynamic thermal loads have a significant effect on the induced strains and the QD. The reported observations can be utilized for optimal design of QD nanostructures thermal loads.

ACKNOWLEDGMENTS

The authors gratefully acknowledge the support by the Slovak Science and Technology Assistance Agency registered under number SK-CN-RD-18-0005.

REFERENCES

Aifantis, E., 1984, On the microstructural origin of certain inelastic models, *ASME J. Eng. Mater. Technol*., 106, 326-330.

Altan, S., Aifantis, E., 1992, On the structure of the mode III crack-tip in gradient elasticity, *Scripta Metall. Mater*., 26, 319-324.

Askes, H., Aifantis, E.C., 2011, Gradient elasticity in statics and dynamics: An overview of formulations, length scale identification procedures, finite element implementations and new results, *Int. J. Solids Struct*., 48, 1962-1990.

Benabbas, T., Francois, P., Androussi, Y., Lefebvre, A., 1996, Stress relaxation in highly strained InAs/GaAs structures as studied by finite element analysis and transmission electron microscopy, *J. Appl. Phys*., 80, 2763-2767.

Bimberg, D., Grundmann, M., Ledentsov, N.N., 1998, *Quantum Dot Heterostructures*, Wiley, New York.

Bishay, P.L., Atluri, S.N., 2012, High performance 3D hybrid/mixed, and simple 3D Voronoi cell finite elements, for macro- & micro-mechanical modeling of solids, without using multi-field variational principles, *CMES: Computer Modeling in Engineering & Sciences*, 84, 41-97.

Chen, X.O., Dong, B., Lei, X.L., 2008, Thermal rectification effect of and interacting quantum dot, *Chin. Phys. Lett*., 25, 3032-3035.

Davies, J.H., Larkin, I.A., 1994, Theory of potential modulation in lateral surface superlattices, *Phys. Rev. B,* 49, 4800.

Davies, J.H., 1998, Elastic and piezoelectric fields around a buried quantum dot: A simple picture, *J. Appl. Phys*., 84, 1358-1365.

DiVincenzo, D.P., 1986, Dispersive corrections to continuum elastic theory in cubic crystals, *Phys. Rev. B*., 34, 5450-5465.

Dong, L., Atluri, S.N., 2011, A simple procedure to develop efficient & stable hybrid/mixed elements, and Voronoi cell finite elements for macro- & micromechanics, *CMC: Computers, Materials & Continua*, 24, 61-104.

Giazotto, F., Heikkil, T.T., Luukanen, A., Savin, A.M., Pekola, J.P., 2006, Opportunities for mesoscopics in thermometry and refrigeration: Physics and Applications, *Rev. Mod. Phys*., 78, 217-274.

Gitman, I., Askes, H., Kuhl, E., Aifantis, E., 2010, Stress concentrations in fractured compact bone simulated with a special class of anisotropic gradient elasticity, *International Journal of Solids and Structures*, 47, 1099-1107.

Glazov, V.M., Pashinkin, A.S., 2000, Thermal expansion and heat capacity of GaAs and InAs, *Inorganic Materials*, 36, 225-231.

Grundmann, M., Stier, O., Bimberg, D., 1995, InAs/GaAs pyramidal quantum dots: Strain distribution, optical phonons, and electronic structure, *Phys. Rev. B,* 52, 11969.

Jogai, B., 2001, Three-dimensional strain field calculations in multiple InN/AlN wurtzite quantum dots, *J. Appl. Phys*., 90, 699.

Liang, X., Shen, S.P., 2013, Size-dependent piezoelectricity and elasticity due to the electric field-strain gradient coupling and strain gradient elasticity, *Int. J. Appl. Mech*., 5, 1350015.

Liao, X.Z., Zhou, J., Cockayne, D.J.H., Leon, R., Lobo, C., 1999, Indium Segregation and Enrichment in Coherent InxGa1-x As/GaAs Quantum Dots, *Phys. Rev. Lett*., 82, 5148-5151.

Liu, Y.M., Yu, Z.Y., Ren, X.M., Xu Z.H., 2008, Self-organized GaN/AlN hexagonal quantum-dots: strain distribution and electronic structure, *Chinese Physics B*, 17, 3471-3478.

Majdoub, M.S., Sharma, P., Cagin, T., 2008, Enhanced size-dependent piezoelectricity and elasticity in nanostructures due to the flexoelectric effect, *Physics Review B*, 77, 125424.

Mindlin, R.D., 1964, Micro-structure in linear elasticity, *Arch. Ration. Mech. Anal*., 16, 51-78.

Pan, E., 2002a, Elastic and piezoelectric fields around a quantum dot: Fully coupled or semicoupled model, *J. Appl. Phys*., 91, 3785-3796.

Pan, E., 2002b, Elastic and piezoelectric fields in substrates GaAs (001) and GaAs (111) due to a buried quantum dot, *J. Appl. Phys*., 91, 6379-6387.

Parton, V.Z., Kudryavtsev, B.A., 1988, *Electromagnetoelasticity, Piezoelectrics and Electrically Conductive Solids*, Gordon and Breach Science Publishers, New York.

Patil, S.R., Melnik R.V.N., 2009, Thermoelectromechanical effects in quantum dots, *Nanotechnology*, 20, 125402.

Pryor, C., Pistol, M.E., Samuelson, L., 1997, Electronic structure of strained InP/Ga0.51In0.49P quantum dots, *Phys. Rev. B*, 56, 10404-10411.

Sladek, J., Sladek, V., Wunsche, M., Tan, C.L., 2017, Crack analysis of size-dependent piezoelectric solids under a thermal load, *Engineering Fracture Mechanics*, 182, 187-200.

Toupin, R.A., Gazis, D.C., 1963, Surface effects and initial stress in continuum and lattice models of elastic crystals. In: Wallis, R.F. (Ed.), *Proc. Int. Conf. on Lattice Dynamics*, Copenhagen, 597-605.

Yaghoubi, S.T., Mousavi, S.M., Paavola, J., 2017. Buckling of centrosymmetric anisotropic beam structures within strain gradient elasticity, *International Journal of Solids and Structures*, 109, 84-92.

MIESZANE SFORMUŁOWANIE MES DLA ANALIZY UKŁADU KROPKI KWANTOWEJ Z WYKORZYSTANIEM TEORII GRADIENTOWEJ

Streszczenie

W pracy opisano analizę nanostruktury kroki kwantowej (QD – ang. Quantum-Dot) poddawanej obciążeniom cieplnym. Wymiary QD są tego samego rzędu co skala długości materiału. Dlatego, aby uwzględnić zależne od wymiaru zachowanie takich nano QD, w analizie należało zastosować gradientową teorię sprężystości. Ponieważ równania opisujące ten problem zawierają pochodne wyższych rzędów niż wymagane w klasycznych rozwiązaniach, do aproksymacji pól w MES należało zastosować elementy C^1. Opracowano mieszane sformułowanie MES, w którym ciągła intermpolacja C^0 jest zastosowana niezależnie do przemieszczeń i gradientów przeieszczeń. Warunki kinematyczne pomiędzy odkształceniami i przemieszczeniami są spełnione poprzez rozmieszczenie specjalnie wybranych punktów wewnątrz elementów. Analizie poddano jednostkową komórkę kropki kwantowej arsenku indu w skończonym obszarze arsenku galu (GaAs).

Received: September 4, 2018.
Received in a revised form: October 13, 2018.
Accepted: November 4, 2018.